BIOCHEMISTRY
including biophysical chemistry & molecular biology

Article

pubs.acs.org/biochemistry

Structure and Mechanism of the Siderophore-Interacting Protein from the Fuscachelin Gene Cluster of *Thermobifida fusca*

Kunhua Li, Wei-Hung Chen, and Steven D. Bruner*

Department of Chemistry, University of Florida, P.O. Box 117200, Gainesville, Florida 32611, United States

Supporting Information

ABSTRACT: Microbial iron acquisition is a complex process and frequently a key and necessary step for survival. Among the several paths for iron assimilation, small molecule siderophore-mediated transport is a commonly employed strategy of many microorganisms. The chemistry and biology of the extraordinary tight and specific binding of siderophores to metal is also exploited in therapeutic treatments for microbial virulence and metal toxicity. The intracellular fate of iron acquired via the siderophore pathway is one of the least understood steps in the complex process at the molecular level. A common route to cellular incorporation is the single-electron reduction of ferric to ferrous iron catalyzed by specific and/or nonspecific reducing agents. The biosynthetic gene clusters for siderophores often contain representatives of one or two families of redox-active enzymes: the flavin-containing "siderophore-interacting protein" and iron−sulfur ferric siderophore reductases. Here we present the structure and characterization of the siderophore-interacting protein, FscN, from the fuscachelin siderophore gene cluster of *Thermobifida fusca*. The structure shows a flavoreductase fold with a noncovalently bound FAD cofactor along with an unexpected metal bound adjacent to the flavin site. We demonstrated that FscN is redox-active and measured the binding and reduction of ferric fuscachelin. This work provides a structural basis for the activity of a siderophore-interacting protein and further insight into the complex and important process of iron acquisition and utilization.

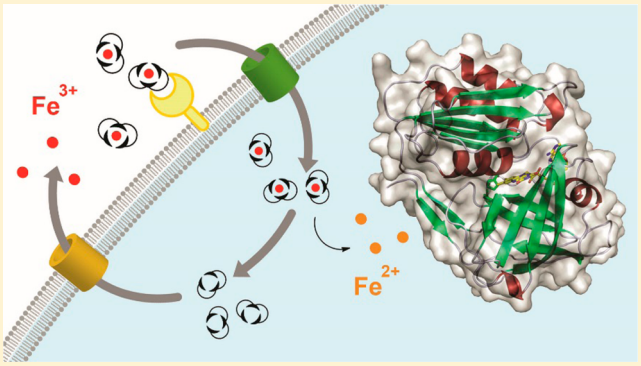

The specific acquisition of elemental iron is essential for a majority of organisms.[1−3] Additionally, the cellular machinery for transporting and assimilating iron often contributes to the virulence of human microbial pathogens.[4−6] Under common aerobic, environmental conditions, ferric iron is poorly soluble and not readily acquirable. Microorganisms have evolved diverse strategies for importing and utilizing iron into key cellular processes.[7] These include direct extracellular reduction of ferric compounds of low solubility to soluble ferrous iron,[8] acquisition of iron-bound heme or heme-containing proteins,[9] removal of metal from host iron-bound transferrin, lactoferrin, or ferritin via specific outer membrane receptors,[10] and production and utilization of small molecule, iron-chelating siderophores.[11,12] Siderophores are secondary metabolites with extraordinary affinity for ferric ions and are utilized as key players in the complex pathways for importing iron. Siderophores are produced in the cytosol or peroxisomes,[13] exported into the extracellular environment, and subsequently imported as a holo-siderophore where the iron is then engaged into the variety of iron-dependent cellular processes.[14]

Siderophores fall into two broad biosynthetic categories, the nonribosomal peptide (NRP)[15,16] and the NRPS-independent siderophore (NIS) pathways.[17] The secondary metabolites have common molecular features that allow extraordinary binding of ferrous iron, including peptide-based scaffolds incorporating metal-chelating functionality as catecholates, hydroxamates, and carboxylates.[12] Specific siderophores are often unique to a producing species, and in addition to utilizing "self"-siderophores, many microbes have the ability to import holo-siderophores produced by other species.[18] Besides iron acquisition, siderophores can also participate in iron storage and intracellular distribution of acquired iron.[19] Several nonclassical biological functions of bacterial siderophores have been identified recently.[20] Moreover, siderophores may also have an influence on the regulation other nonbacteriostatic mammalian processes.[21,22] Because of the importance of the process, various siderophore pathway-based therapeutical applications have been developed during the past decades. Therapeutic iron chelators with siderophore scaffolds have been used in the treatments of blood transfusion-requiring diseases such as β-thalassemia.[23,24] Antibiotic/siderophore conjugates have been developed as potential drug leads with reduced permeability-mediated drug resistance using a "Trojan Horse"-type mechanism.[25−27] Additionally, interruption of siderophore recycling is a potential therapeutic approach.[28−30]

Received: April 3, 2015
Revised: June 2, 2015
Published: June 4, 2015

DOI: 10.1021/acs.biochem.5b00354
Biochemistry 2015, 54, 3989−4000

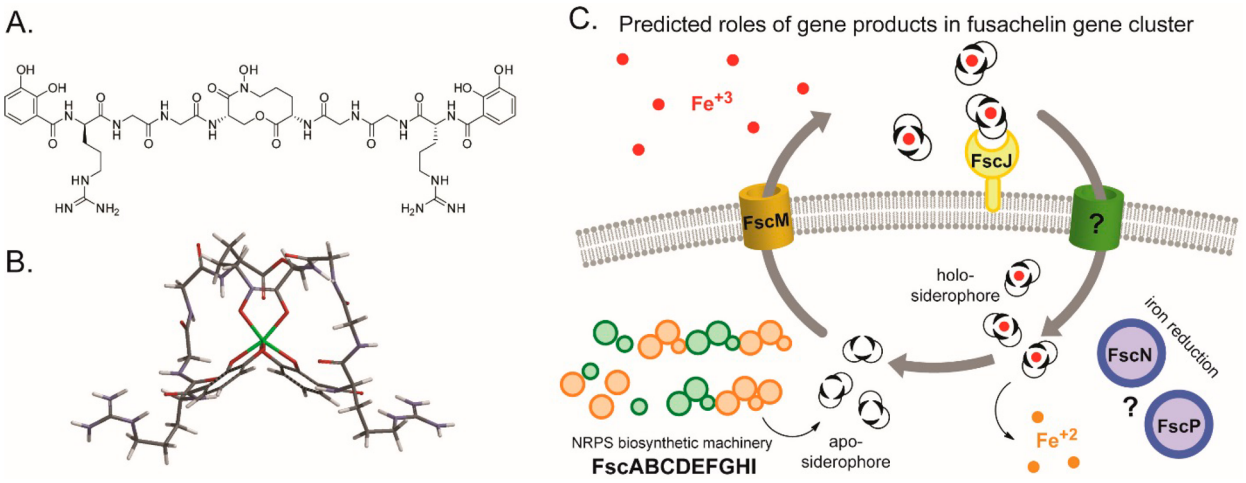

Figure 1. Fuscachelin siderophore pathway of *T. fusca*. (A) Structure of the nonribosomally based peptide siderophore fuscachelin A along with (B) a three-dimensional model of the fuscachelin A–iron (green) complex. (C) Schematic diagram showing the predicted roles of genes in the *T. fusca* siderophore gene cluster.

The overall pathway for siderophore-based iron acquisition has been studied well, and many of the players and mechanisms are established.[31] Intracellular siderophore production likely occurs in the proximity of the cellular membrane and is coupled to export.[32] Export and import of apo-siderophore/iron-siderophore across the cellular membrane(s) have been studied in both Gram-positive and Gram-negative bacteria. For Gram-positive bacteria, these include the EntS-type major facilitator superfamily (MFS) exporter and import through a FepCDG-like multifunctional ABC transporter system associated with a FepB-like transporter through the ligand exchange mechanism.[33−35] Imported ferric iron bound to a siderophore must be released to be made available to cellular machinery. One strategy for iron release is through hydrolytic destruction of the siderophore by esterases of the α,β-hydrolase family of enzymes, represented by the *Escherichia coli fes*, *iroD*, and *iroE* gene products, which is a common strategy for macrolactone-based siderophores.[36,37] For non-ester-containing siderophores, iron release is commonly proposed to be facilitated by single-electron reduction of the ferric siderophore to the ferrous oxidation state, allowing kinetic exchange with downstream iron-chelating sites found in cellular protein or small molecules.[38]

There are multiple proposed routes for the intracellular iron reduction and mobilization into an accessible iron pool. Among the paths, the reduction of ferric-siderophores is proposed to occur through a flavin-dependent electron transport via a specific or nonspecific mechanism. A nonspecific reduction path could also proceed alongside the cleavage or hydration of siderophores through canonical endogenous reducing reagents such as ascorbate or thiols.[39] In several pathways, iron-siderophore-specific reduction is proposed and genes for reductases are clustered with the genes for siderophore biosynthesis and transport. The enzymology of specific iron reduction has been studied in limited systems, one being the *E. coli* flavoreductase, YqjH.[40]

The protein superfamily that includes YqjH is termed the "siderophore-interacting protein" (SIP) family. A preference of NADPH for reduction of bound flavin has been demonstrated for YqjH, along with the ability to reduce diverse iron chelates, including ferric enterobactin.[40] The *ygjH* gene is a part of the Fur regulon and under transcriptional control of *yqjI*, a winged helix transcriptional regulator.[41,42] Interestingly, the DNA binding of YqjI is dependent on Ni^{2+} binding (not iron), and it is proposed that the gene product helps regulate iron acquisition under conditions that include high nickel ion concentrations, which can disrupt iron homeostasis.[43] A second class of specific intracellular reductases contain an Fe–S cluster as exemplified by *E. coli* FhuF [termed the ferric siderophore reductase (FSR) family]. FhuF is part of the siderophore-reductase system with a sufficient redox potential to reduce ferric ferrioxamine. This class contains a unique C-terminal C-C-x_{10}-C-x_2-C iron–sulfur cluster binding motif that does not show significant similarities to other known [2Fe-2S] proteins.[44] The homologous FchR from *Bacillus halodurans* DSM497 has been reported to work in a three-component electron donor system, along with NADPH and ferredoxin, to reduce various iron chelates with optimal demonstrated reduction activity against ferric dicitrate.[45] We have previously characterized a novel siderophore-producing biosynthetic gene cluster in the actinomycete *Thermobifida fusca* along with the structure of the unique metabolite (Figure 1A,B).[46,47] The nonribosomal peptide (NRP) fuscachelin is a mixed catecholate/hydroxamate with several unique structural features. The gene cluster for fuscachelin contains many of the commonly found components for iron acquisition (Figure 1C and Table S1 of the Supporting Information). The biosynthetic machinery includes NRP synthetases (FscFGHI) and accessory biosynthetic enzymes FscABCDEK, in addition to genes for transport and iron utilization. FscM is homologous to EntS-siderophore transporters and is likely involved in export of the apo-siderophore. FscJ is a membrane-anchored siderophore binding protein proposed to bind and deliver the ferri-siderophore to the ABC transporter system. There are no genes for an ABC transporter system specific to the fuscachelin gene cluster; however, examination of the *T. fusca* genome suggests a cluster (*tfu_0336–0338*) as a likely candidate with homology to the *E. coli* FepCDG/FhuCB machinery.[48] These three genes are regulated by DtxR, an iron-dependent transcriptional repressor that controls the expression of siderophore gene clusters in *T. fusca*.[49] We are interested in exploiting the thermostability inherent in *T. fusca* to characterize the structure and mechanisms of the complex machinery

DOI: 10.1021/acs.biochem.5b00354
Biochemistry 2015, 54, 3989–4000

involved in siderophore biosynthesis and iron acquisition/utilization.

Representatives of the two proposed families involved with intracellular iron reduction are present in the *T. fusca* cluster. FscN is a flavoprotein of the SIP family, and FscP is a member of the FSR family that shares a high degree of homology of its Fe−S cluster with *E. coli* FhuF. It is uncommon to find representatives of both protein classes in a single siderophore gene cluster. There are limited structural data available to provide a basis for the function of either superfamily in siderophore utilization. For the SIP family, there is a preliminary X-ray diffraction analysis of YqjH from *E. coli* (without structural determination),[50] and a structure of a homologue from *Shewanella putrefaciens* has been determined and deposited (PDB entry 2GPJ) as part of the Joint Center for Structural Genomics.[51] The 2.2 Å structure of the *S. putrefaciens* protein establishes the SIP class as a member of the broad flavoreductase family with N-terminal β-barrel and C-terminal $\alpha/\beta/\alpha$ sandwich domains form the unique structural clades present in the SIP family across bacterial species.[40] There are no structures available (or significant structural homologues) for the FSR family of reductases. Here we report the structure and biochemical characterization of FscN as a flavin-dependent iron reductase. The results provide a structural basis for SIP function and insight into siderophore utilization in Gram-positive bacteria.

EXPERIMENTAL PROCEDURES

General Methods. Unless otherwise stated, reagents and chemicals were purchased from Fisher Scientific or Sigma/Aldrich.

Cloning, Expression, and Purification of FscN. The gene for *fscN* was amplified via polymerase chain reaction (PCR) from *T. fusca* (ATCC 27730) genomic DNA with the following primers: FscN_Nterm (5′-GCG GGA TCC ATC ACC GCA ACC GTG) and FscN_Cterm (5′-GCG AAG CTT CTA CTC GTC GTC ATC GTC). The PCR products were purified through agarose gel electrophoresis and cleaved with the corresponding restriction endonucleases. The resultant *fscN* gene was then ligated into expression vector pET28a and transformed into *E. coli* BL21(DE3)pLysS cells for expression. Cultures (1 L) were grown to an OD_{600} of 0.6−0.8 at 37 °C, and overexpression was initiated by the addition of 100 μM IPTG and growth continued for 16 h at 16 °C before the cells were harvested by centrifugation. Cell pellets were resuspended in 25 mL of 20 mM Tris-HCl (pH 7.5) and 0.5 M NaCl and lysed at 14000 psi through a nitrogen-pressure microfluidizer cell (M-110L Pneumatic). The lysate was clarified by centrifugation at 10000*g* for 40 min at 4 °C. FscN was purified using metal affinity chromatography (HisPur Ni-NTA Resin, Thermo Scientific). After being bound for 1 h, the resin was washed with 4 × 10 mL of 20 mM Tris-HCl (pH 7.5), 0.5 M NaCl, and 25 mM imidazole, and the bound protein was eluted with 3 × 4 mL of wash buffer with 250 mM imidazole. The resulting yellow elution solution was dialyzed against 1 L of 20 mM Tris-HCl (pH 7.5) and 100 mM NaCl for 16 h and further purified with a HiTrapQ HP anion exchange column (column size of 5 mL, GE Healthcare, AKTA FPLC System) and HiLoad 16/60 SuperDex-200 gel filtration chromatography (GE Healthcare). To rule out contaminating Ni^{2+} from Ni^{2+}-NTA-based purification, an alternative protein purification strategy using ammonium sulfate precipitation (ASP) was also used for ICP-MS analysis. Briefly, the cell pellet was resuspended and lysed as described above, and ammonium sulfate was added to the supernatant and the concentration increased stepwise (10, 30, 50, and 80% saturation). For each step of addition, ammonium sulfate was gently added to the tube over 5 min and rocked for an additional 5 min to facilitate dissolution. When all of the ammonium sulfate was dissolved, the tube was placed on ice for 30 min to allow further precipitation of protein before the precipitant was harvested via centrifugation (3000*g* for 10 min at 4 °C). The precipitant was resuspended in 5 mL of 20 mM Tris-HCl (pH 7.5) and analyzed at each stage, and the target protein was recovered in the 50% precipitant fraction. The protein was dialyzed and further purified by anion exchange and gel filtration chromatography as described above for Ni-NTA-purified protein.

FAD Determination, Reduction, and Enzyme Kinetics. To determine the cofactor composition, purified FscN was denatured by being heated at 95 °C for 20 min. After the precipitate had been removed by centrifugation, the supernatant was analyzed by LC−MS (Agilent 6130, SB-C18 column) with a gradient from 2 to 98% CH_3CN in aqueous 0.1% TFA over 17 min at a flow rate of 1 mL min^{-1}. Preparative HPLC (GraceVydac C18) purification was conducted with a linear gradient from 3 to 40% methanol in aqueous 0.1% TFA over 30 min at a flow rate of 10 mL min^{-1}. Detection wavelengths of 320 and 460 nm were chosen to monitor the elutions. The m/z 784 peak in LC−MS represents FAD as cofactor.

Reduction of the FAD cofactor *in vitro* was assayed as described previously.[50] FscN at a concentration of 1.5 mg/mL in a 1 cm cuvette was reduced by addition of an excess of sodium hydrosulfite, and the spectrum was subsequently recorded at 16 min intervals (16, 32, 48, 64, and 80 min). A detection wavelength of 459 nm was selected to assess FAD reduction.

The FscN-catalyzed reduction assay was performed anaerobically in 100 mM potassium phosphate buffer (pH 7.5) at 37 °C. For substrates ferric-EDTA, ferric chloride, ferric citrate, ferricyanide, and ferric 2,3-dihydroxybenzoic acid, the enzyme concentration was set at 10 μM with the NADH concentration from 0.5 to 2.0 mM; 0.6 mM ferrous indicator 3-(2-pyridyl)-5,6-bis(2-furyl)-1,2,4-triazine (ferene) was added to monitor the formation of ferrous ion by measuring the absorbance at 595 nm. For substrates ferric enterobactin and ferric fuscachelin A, because of the self-absorbance change of the $Fe^{2+/3+}$−siderophore complex near 600 nm, reactions were monitored through the concentration change of reactant NADH with a detection wavelength of 340 nm. The final concentrations of enzyme, NADH, and substrate were set at 10 μM, 0.1 mM, and 0.2 mM, respectively, and the reaction rate was calculated using a NADH ε_{340} of 6220 M^{-1} cm^{-1}.

Purification of the Ferric-Fuscachelin Complex. Apo fuscachelins A−C were produced from a *T. fusca* culture as previously reported with modifications and identified correspondingly.[47] Briefly, *T. fusca* spores (ATCC 27730) were cultured in 5 mL of LB broth at 55 °C while being shaken at 150 rpm overnight, and then cells were fully exchanged into 5 mL of iron-deficient Hägerdal medium before inoculation with 1 L of iron-deficient Hägerdal medium and growth was continued for 7 days at 55 °C. Cell pellets were collected by centrifugation and extracted with methanol. The methanol extracts were concentrated and subjected to preparative HPLC by using a Vydac 218TP1022 protein and peptide C18 column

DOI: 10.1021/acs.biochem.5b00354
Biochemistry 2015, 54, 3989−4000

(250 mm × 22 mm, 10 μm). A linear gradient from 2 to 50% methanol in 0.1% TFA and water was run over 30 min at a rate of 10 mL min^{-1}, and fractions collected at 17.6, 18.2, and 19.1 min were confirmed to be fuscachelin C, B, and A, respectively. Purified fuscachelin A was incubated with ferric ammonium sulfate in a 1:10 ratio, and the resulting ferric fuscachelin A complex was purified using preparative HPLC with a linear gradient from 3 to 80% methanol in 5 mM NH_4OAc over 25 min at a rate of 10 mL min^{-1}. Apo-fuscachelin A with an elution time of 11.2 min was converted quantitatively into holo-fuscachelin A with an elution time of 14.6 min (Figure S1 of the Supporting Information).

Metal Analysis. The hexahistidine tags of purified FscN from both nickel NTA affinity chromatography and ammonia sulfate precipitation were removed using a standard thrombin cleavage protocol. Briefly, 1 μL of thrombin (1 unit μL^{-1}, Novagen) was mixed with 10 mg of protein in 1 mL of thrombin cleavage buffer [20 mM Tris-HCl, 150 mM NaCl, and 2.5 mM $CaCl_2$ (pH 8.4)] and incubated for 16 h at room temperature. Cleaved protein was further purified using size exclusion chromatography (as described above). FscN-containing fractions (8 mL) were dialyzed against 1 L of metal-free 0.1 M ammonium acetate (pH 6.5) for 16 h [pretreated with 5% (w/v) Chelex 100 Resin for 4 h] and diluted with the same buffer to 10 mL (0.3 mg/mL). Concentrated nitric acid (trace metal grade, Sigma) was then added to a final concentration of 1%. A blank 10 mL reference was also prepared in parallel using identical procedures. Samples were analyzed with inductively coupled plasma mass spectrometry (ICP-MS) at the Center for Applied Isotope Studies of the University of Georgia (Athens, GA). Cu, Zn, Mn, Mg, Ni, Co, and Fe were analyzed for each sample along with the blank reference.

Crystallography, Structure Determination, and Refinement. Initial crystal screening for FscN was performed in sitting drop format with commercial matrix screens (Hampton Research). Optimization of initial conditions gave rod-shaped crystals with approximate dimensions of 400 μm × 100 μm × 100 μm using a reservoir solution consisting of 0.95 M ammonium sulfate, 0.1 M Tris-HCl (pH 6.6), and 35% (v/v) 2-methyl-2,4-pentanediol (hanging drop method, room temperature). Typically, crystals appeared in 4 weeks and grew to maximal dimensions in 8−10 weeks. Crystals suitable in size were harvested and frozen in liquid nitrogen using additional 30% glycerol as a cryoprotectant. Diffraction data were collected at the PXRR X25 beamline at Brookhaven National Laboratories (Upton, NY) National Synchrotron Light Source and processed with XDS[52] to a resolution of 1.89 Å in space group *C*2 (Table 1). The asymmetric unit contains two molecules of FscN. Deposited SIP protein from *S. putrefaciens* (PDB entry 2GPJ, 32% sequence identity) was used as a starting model for molecular replacement in phaser.[53] Refinement was performed in phenix.refine[54] in PHENIX 1.7.1,[55] and model building was performed using COOT.[56] On the basis of the refined model, the sigma-weighted, simulated composite omit maps and anomalous difference electron density maps were calculated with phenix.maps.[55] Graphical representations were prepared with PyMOL.[57] Several independent PCRs and sequencing confirmed that the construct of *fscN* from *T. fusca* ATCC 27730 deviates from the published genome of *T. fusca* strain YX at one codon: position 99 is an Arg (AGA) in ATCC 27730 and a Gly (GGA) in *T. fusca* strain YX. Arg99 is located on the surface of the resolved structure of FscN and is outside the active site.

Table 1. X-ray Crystallography Statistics of the Complex of FscN with FAD

	Data Collection[a]
wavelength (Å)	1.100
resolution range (Å)	36.74−1.89 (1.96−1.89)
space group	C121
unit cell dimensions (Å)	129.54, 75.07, 73.90, 90, 102.62, 90
total no. of reflections	199130 (17743)
no. of unique reflections	54927 (4941)
multiplicity	3.4 (3.3)
completeness (%)	98.95 (94.18)
mean $I/\sigma(I)$	12.81 (2.64)
Wilson *B* factor	26.66
R_{merge}	0.0587 (0.44)
R_{meas}	0.0686
CC1/2	0.998 (0.899)
	Refinement
R_{work}/R_{free}	0.189/0.219
no. of atoms	4643
protein	4141
ligand	140
water	362
no. of protein residues	523
root-mean-square deviation	
bond lengths (Å)	0.007
bond angles (deg)	1.31
Ramachandran plot	
favored (%)	99
outliers (%)	0
Clashscore	3.79
average *B* factor	35.20
protein	35.30
ligand/ion	29.30
water	37.20
PDB entry	4YHB

[a]Data values for the highest-resolution bin (1.96−1.89 Å) are shown in parentheses.

RESULTS

FscN Contains a Noncovalently Bound FAD Cofactor. The *fscN* gene was cloned from *T. fusca* ATCC 27730 genomic DNA, and the protein was purified as a hexahistidine fusion using standard chromatographic techniques. The purified protein was bright yellow, indicative of a bound flavin-type cofactor. The UV−visible spectrum of the isolated protein was consistent with flavin adenine dinucleotide (FAD) in the oxidized form, with the absorption maxima at 388 and 459 nm and distinct shoulders located at 459 and 481 nm (Figure 2A). To further identify the cofactor, the purified protein was denatured at high temperatures and the yellow supernatant was analyzed via LC−MS, resulting in a molecular weight of 785.55 Da corresponding to the UV-active component, supporting FAD as the isolated cofactor (Figure 2A). The protein precipitate formed during the denaturation appeared white and was not UV-active, suggesting the cofactor is bound to protein through a noncovalently or labile covalent interaction. To confirm that the FAD cofactor was redox-active in the context of FscN, the protein was reduced by sodium dithionite under anaerobic conditions.[58] During the reaction, the magnitude of the 459 nm shoulder decreased, suggesting the disappearance of FAD over time, while the increase in the

DOI: 10.1021/acs.biochem.5b00354
Biochemistry 2015, 54, 3989−4000

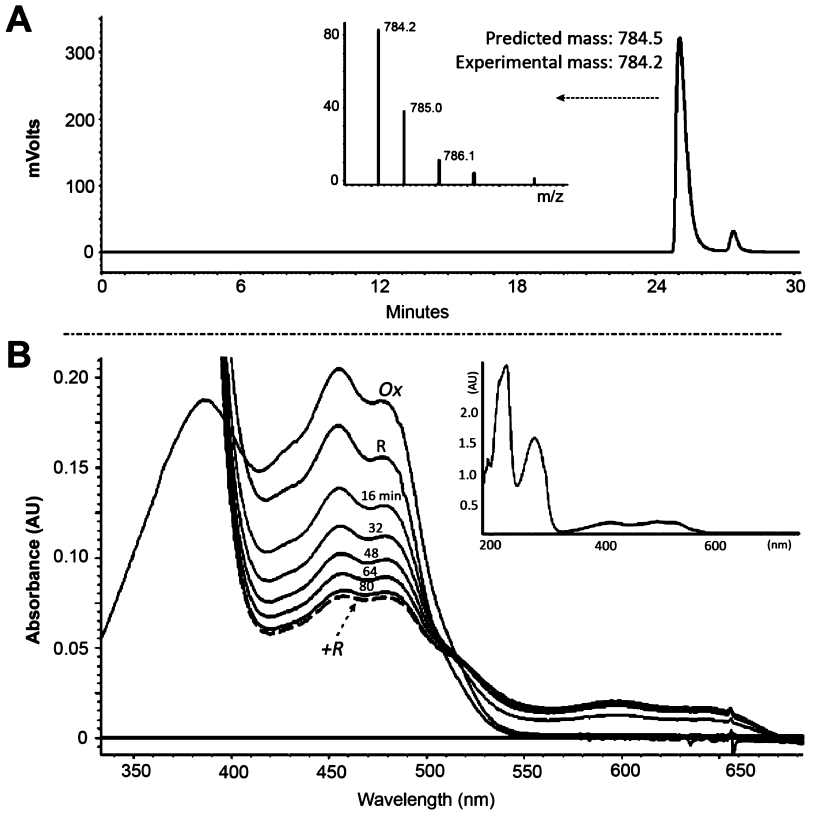

Figure 2. Properties of the cofactor flavin-bound FscN. (A) LC−MS analysis of the purified flavin cofactor, confirming the cofactor identification as noncovalent bond FAD. (B) UV−visible spectra of FAD bound (*Ox*) along with time points (16, 32, 48, 64, and 80 min) of reduction with sodium dithionite to $FADH_2$ (+*R*, dotted line). The inset shows the full spectrum of reduced protein.

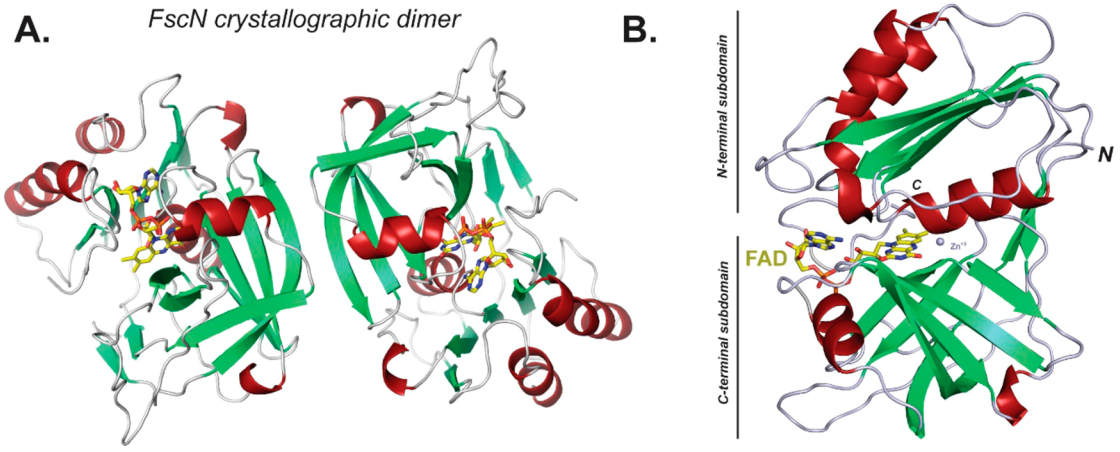

Figure 3. X-ray crystal structure of FscN. (A) Dimer present in the asymmetric unit shown in ribbon format with the flavin cofactor in licorice representation. (B) One monomer of FscN illustrating the two N- and C-terminal subdomains and the location of an observed bound metal (shown as a Zn^{2+} ion).

magnitude of the 600 nm shoulder peak indicates the formation of reduced $FADH_2$ (Figure 2B).

The Siderophore Utilization Protein FscN Shows Binding Affinity for Ferric-Fuscachelin. Isothermal titration calorimetry (ITC) supports binding of FscN to ferric-fuscachelin A with a reasonable binding affinity. FscN was titrated against ferric-fuscachelin A, and an overall binding mode was modeled as an enthalpy-driven process with a calculated binding affinity (dissociation constant) of 30 μM (Figure S3 of the Supporting Information). We tested several other ferric-siderophores for binding to FscN to determine the specificity of FscN. Ferric-EDTA, ferric-citrate, and ferric-2,3-dihydroxybenzoic acid (DHB) were all tested using identical ITC conditions, and no significant binding affinity was observed.

FscN Specifically Reduces Ferric Fuscachelin. Ferric reductase assays were performed anaerobically in a phosphate buffer to further address the bioactivity of FscN.[40] Purified FscN showed no ferric reductase activity toward ferric chloride, ferric-EDTA, ferric citrate, ferric 2,3-dihydroxybenzoic acid, or the ferric enterobactin complex (data not shown). Relatively weak activity (40 nmol of Fe^{2+} min^{-1} mg^{-1}) toward purified

DOI: 10.1021/acs.biochem.5b00354
Biochemistry 2015, 54, 3989−4000

ferric-fuscachelin A was detected in the presence of NADH (Figure S4 of the Supporting Information). The range of activity is consistent with that previously reported for YqjH, which was reported to be 22.0 nmol of Fe^{2+} min^{-1} mg^{-1} with a K_M of 33 μM.[41] In contrast to YqjH, inclusion of NADPH in the reaction mixture in place of NADH did not result in any observable reduction, suggesting that FscN functions as a NADH-dependent ferric siderophore reductase.

Structure Determination via X-ray Crystallography. FscN protein crystals diffracted in space group *C*2, and the structure was determined using the deposited structure of the SIP from *S. putrefaciens* (PDB entry 2GPJ) as a molecular replacement search model. The final model was refined to 1.89 Å resolution with two monomers of FscN present in the asymmetric unit (Figure 3 and Table 1). The observed dimer is most likely a result of crystal packing and does not represent the biological unit based on analysis of the interface using the PISA server,[59] and the size exclusion chromatography elution profiles are consistent with an FscN monomer (Figure S5 of the Supporting Information). The two monomers in the asymmetric unit are highly similar, with a total atom rmsd of 0.26 Å, and the following discussion and figure representations will refer specifically to deposited monomer A.

The overall molecular structure of FscN consists of two subdomains: an N-terminal FAD binding domain and the C-terminal NADH binding domain that are connected by a linker region consisting of a two-strand β-sheet. The cofactor FAD is clearly resolved in the electron density maps and noncovalently bound in the boundary cleft between the two major domains. The FAD binding domain has six antiparallel β-strands with a small α-helix connecting a long loop. The arrangement of the NADH binding domain forms a $\beta1-\alpha-\beta2$ architecture as is typical of the NAD(P)H binding motif common to the classic Rossmann fold.

FscN displays significant structural homology to the diverse family of FAD/NAD(P)H oxidoreductases. Using the structural homology program Dali,[60] several NAD(P)H/ferridoxin reductases show *Z* scores in the modest range of 17−19 with overall sequence identity between 10 and 15%. The highest overall degrees of similarity are with flavohemoglobins (see Table S4 of the Supporting Information), three domain proteins that contain an iron-heme domain in addition to the two ferridoxin-reductase subdomains common to FscN.

The FAD cofactor is bound in a typical conformation as seen with examples from this superfamily (Figure 4). The negatively charged FAD diphosphate group is stabilized largely via hydrogen binding interactions with His108 and Ser261. The isoalloxazine ring of flavin is bound through aromatic stacking interactions among Tyr255, His53, Tyr89, and His265. Additionally, an aromatic stacking arrangement holds the adenine moiety between Trp256 and His108, and hydrogen bond interactions between the FAD and the protein are seen with the 2′-hydroxyl of the ribose and the exocyclic amino of the adenine to further reinforce the protein−cofactor interaction.

Proposed NADH Cofactor Binding Site in FscN. The presented structure is in a "closed" conformation where the C-terminus is occupying the likely NADH binding site. This is a common structural rearrangement observed in this reductase class, and the PDB database is represented by both NAP(P)H-bound and unbound states. In the ferridoxin reductase superfamily, two electrons are commonly transferred from NAD(P)H to oxidized flavin followed by transfer to an

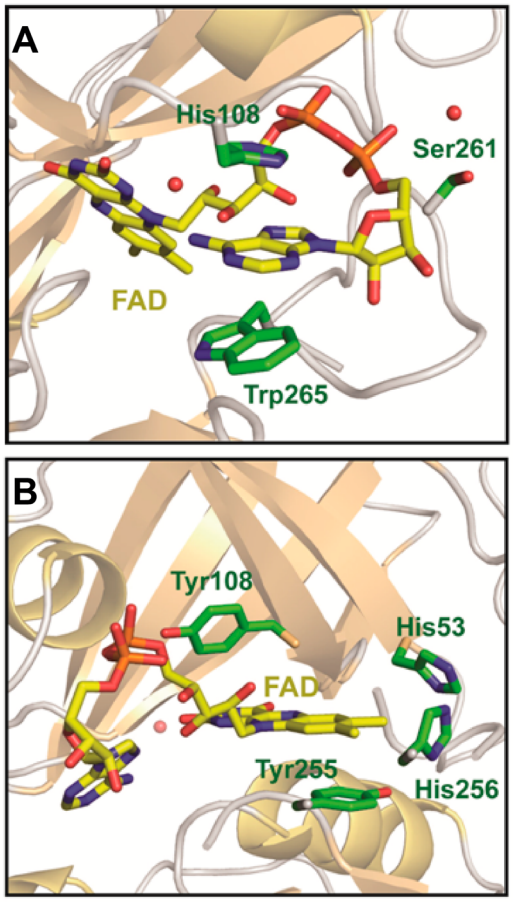

Figure 4. Two views of the flavin binding site illustrating key residues involved with cofactor interaction.

additional electron acceptor. In FscN, the NADH binding site is at the interface of the two domains and can bind only while the protein is in an "open" conformation. Overlaying the structure of FscN with NADH-cytochrome b_5 reductase[61] [PDB entry 3W2G (Table S4 of the Supporting Information)] allows insight into the predicted NADH binding to FscN to be gained. The open structure NADH-cytochrome b_5 reductase has the nicotinamide stacked with the flavin isoalloxazine, in a position consistent with electron transfer. This stacking position in FscN is occupied by Tyr255 at the C-terminus, and disordering and/or displacing of the terminus would need to accompany NADH binding. The structural arrangement has the common features consistent with an established ping-pong, bi-bi mechanism of NADH oxidation and substrate binding/reduction.[62] Residues observed to bind the NADH cofactor in cytochrome b_5 reductase are conserved in FscN, suggesting a similar binding mode (see Figure 6A). In contrast to *E. coli* YqjH, with reported activity using NADPH as a cofactor, FscN has a longer loop between $\beta12$ and $\alpha3$ to bind the adenine part of the cofactor (see Figure 5). Structural homologues determined to have different cofactor affinity also have slightly different sequence characteristics in this region. Enzymes that utilize NADPH have a relatively shorter loop, while NADH-dependent proteins commonly have a longer loop with the notable presence of negatively charged residues.[63,64] Previous research also suggests that negatively charged amino acids (residue Glu173 in FscN) located on this loop interact with the adenosine ribose moiety and decrease NADPH affinity,

DOI: 10.1021/acs.biochem.5b00354
Biochemistry 2015, 54, 3989−4000

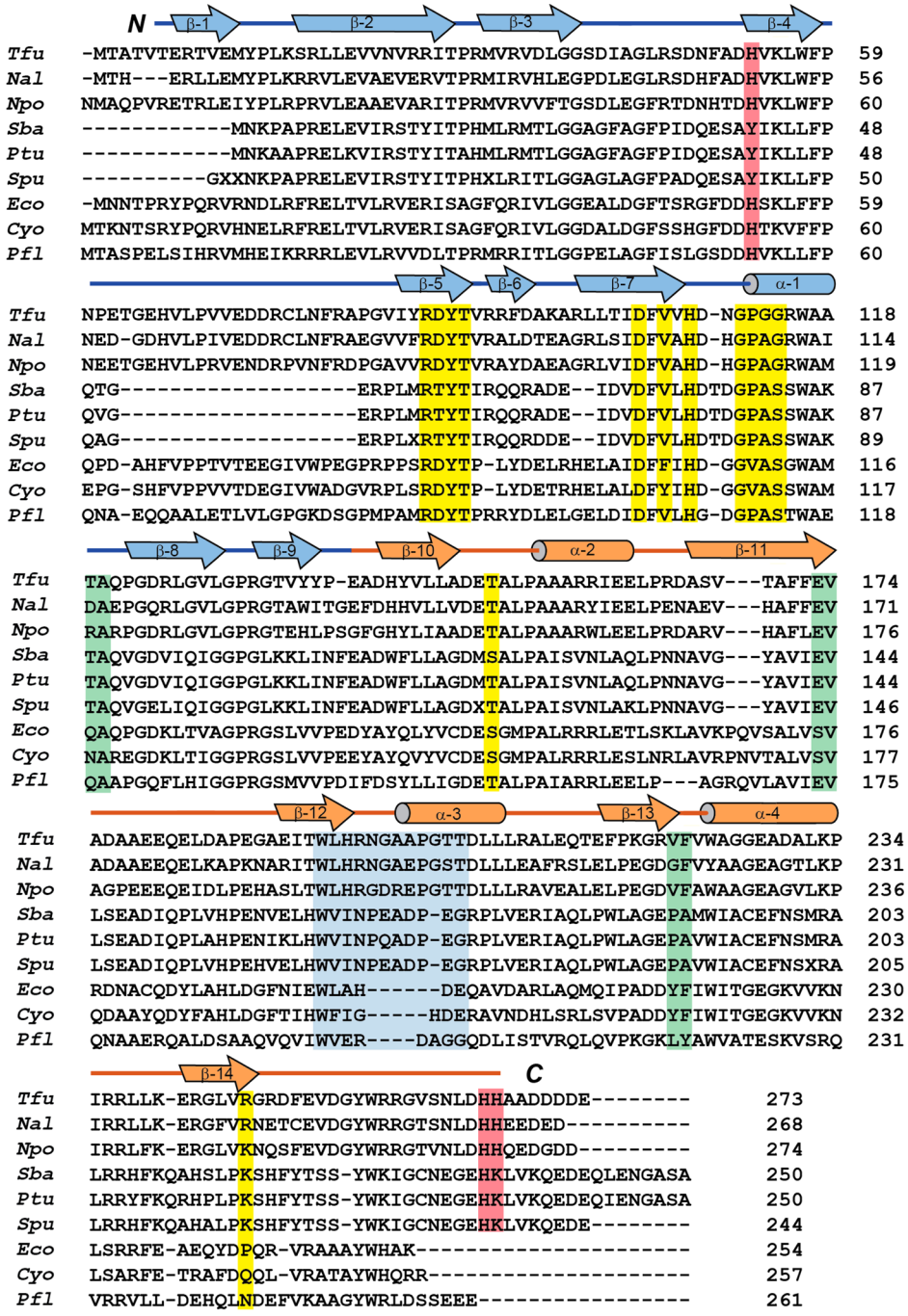

Figure 5. Global multiple-protein sequence alignment of putative SIP proteins. Subgroups with differences in the N- and C-terminal regions are clustered. Conserved residues with green for the NAD(P)H binding motif, yellow for the FAD binding pocket, and red for residues associated with putative metal binding. Abbreviations: Tfu, *T. fusca*; Nal, *Nocardiopsis alba*; Npo, *Nocardiopsis potens*; Sba, *Shewanella baltica*; Ptu, *Pseudoalteromonas tunicata*; Spu, *S. putrefaciens*; Eco, *E. coli*; Cyo, *Citrobacter youngae*; Pfl, *Pseudomonas fluorescens*.

enhancing the ability to utilize NADH.[65] The structural analysis along with the kinetic assays is consistent with FscN serving as a reductase with cofactor specificity for NADH.

Metal Binding Site Adjacent to the Flavin Cofactor. From the calculated electron density maps, there is a pronounced metal site adjacent to the hydrophobic side of the flavin binding pocket (Figure 6B and Figure S6 of the Supporting Information). The calculated anomalous difference map shows a strong peak at a 15σ contour level, with a wavelength of 1.100 Å. The electron density at the metal site is present at a contour level of up to 12σ in $2F_o - F_c$ map (Figure 6B), indicating the high occupancy of a heavy atom. The metal ion is coordinated by three histidines, His53, His255, and His256, with nitrogen−metal distances of 2.18, 2.17, and 2.16 Å, respectively. Three water molecules also surround the metal center with distances of 2.18, 2.18, and 2.27 Å giving a six-coordinated metal center with ideal octahedral geometry. To identify the metal bound to FscN, ICP-MS analysis of the IMAC-purified protein sample resulted in Ni^{2+} or Zn^{2+} [0.8 and 0.25 molar ratios, respectively (Table S5 of the Supporting Information)]. To exclude the possible influence of an external metal ion from the Ni^{2+}-NTA resin used for protein

DOI: 10.1021/acs.biochem.5b00354
Biochemistry 2015, 54, 3989−4000

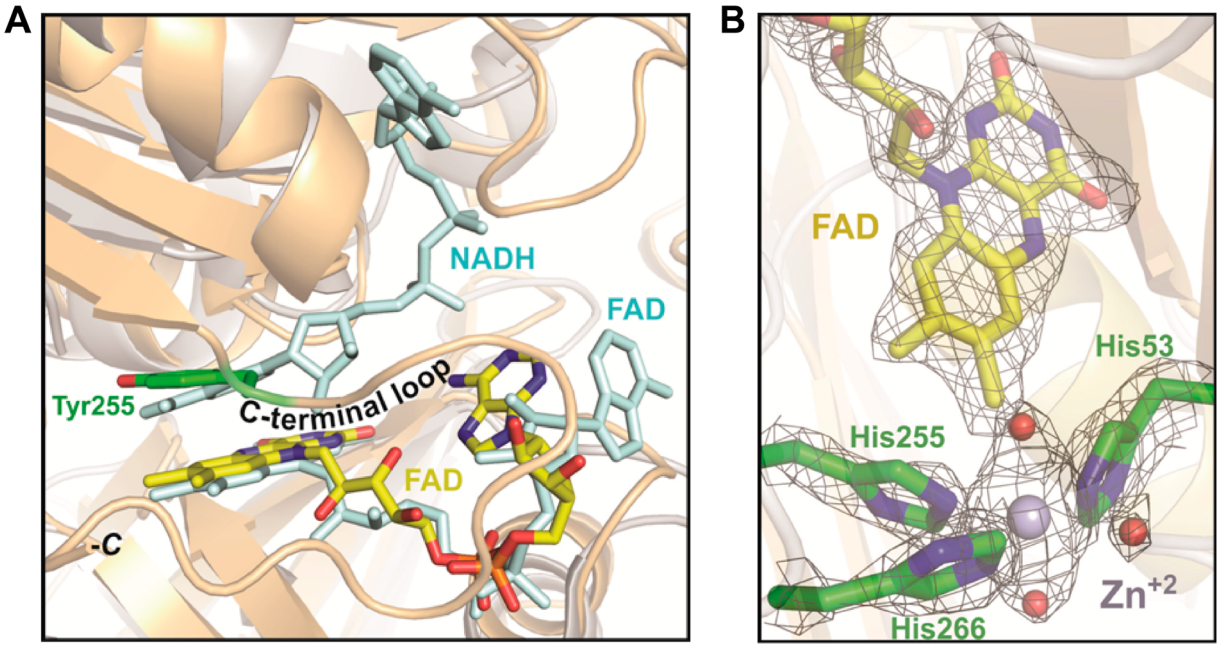

Figure 6. (A) Overlaying the structure of FscN (wheat) with NADH-cytochrome b_5 reductase (light blue). (B) Metal binding site adjacent to the hydrophobic side of the flavin binding pocket in FscN. $2F_o - F_c$ electron density map is calculated at 1.5σ.

purification, further analysis was conducted with the protein purified through ammonium sulfate precipitation. Analysis of this sample resulted in an FscN:Ni^{2+}:Zn^{2+} ratio of 1:0.22:0.80, indicating a predominant Zn^{2+} form; however, the 0.22 molar ratio of Ni^{2+} is not insignificant, beyond that expected for background.

DISCUSSION

Presented is the first structure coupled with functional characterization of a SIP flavoenzyme. The fate of iron-siderophores after import into cells is a complex and important step in bacterial iron acquisition. The study of the overall process provides basic biochemical insight into the complex molecular machinery and can provide details into virulence mechanisms. The fuscachelin siderophore biosynthetic gene cluster encoded in the genome of the moderate thermophile *T. fusca* is a useful model system for studying the overall mechanism. All common genes, including those for siderophore peptide biosynthesis, export and import, and utilization, are present in the cluster, including representatives implicated in intracellular iron reduction, the SIP, FscN, and the FSR, FscP. Iron is imported into *T. fusca* complexed with a siderophore in the oxidized ferric form and is at some point reduced to the ferrous state for uptake by cellular machinery. There have been limited published biochemical characterizations of intercellular siderophore iron reduction. As discussed, several pathways have been proposed, including extracellular reduction and non-specific intracellular reduction paths. A majority of bacterial siderophore gene clusters contain one representative of either the SIP or FSR superfamily proteins. The FSR family is represented by *E. coli* FhuF, a ferredoxin homologue containing an uncommon C-C-$x_{10/11}$-C-x_2-C binding motif, which shares limited sequence similarity to other characterized 2Fe-2S ferridoxins. Examples from both families have recently been reported to reduce iron-siderophores *in vitro*: FchR reduction of ferric dicitrate[45] and SIP YqjH reduction of ferric enterobactin.[40] It is not clear if these functions are redundant or synergistic in siderophore pathways.

The *fscN* gene is part of the siderophore gene cluster of *T. fusca*. FscN is a member of the SIP family and homologous to ViuB, required for siderophore utilization in *Vibrio cholerae*.[66] This family functions as NAD(P)H:flavin oxidoreductases, and homologues are found to be widely distributed in bacteria. Two different subfamilies of SIPs can be distinguished, primarily on the basis of C-terminal sequence alterations.[67,68] Group I (Figure 5), including FscN from *T. fusca*, contains an additional 15−20 amino acids predicted to be a C-terminal α-helical elements with a conserved HH(K)x_5DE sequence. In contrast, group II, represented by *E. coli* YqjH, has a relatively shorter C-terminus. All sequences have highly conserved flavin cofactor binding motifs, including RxYT, DxV(F)xH, Gx_2S, and YWK(R) highlighted in yellow (Figure 5). As compared to group II SIPs, group I SIPs have a more conserved NAD(P)H binding motif (TA-x_3-EVL-x_3-GE) (colored green). The NAD(P)H motif, QA-x_3-SVL, common to group II is less common. Consistent with bioinformatics analyses, the group I YqjH uses NADPH, whereas in this report, we demonstrate that the group II FscN utilizes NADH as a reducing agent.

The structure of FscN contains a flavin cofactor bound in an overall conformation typical of flavoreductases, with the isoalloxazine ring in a planar configuration indicative of oxidized FAD (Figure 6). The dinucleotide is in an extended orientation with the terminal adenosine at the surface of the protein. The identity of the cofactor was determined by protein denaturation followed by spectroscopic characterization of the isolated cofactor. These, in combination with the presented structure, clearly suggest a noncovalently bound flavin. This is contrast to the reported characterization of the *E. coli* homologue, YqjH, in which the cofactor was suggested to be covalently bound. Covalently bound flavin is commonly linked through the C6 atom or/and the 8-methyl on the isoalloxine ring through cysteine, histidine, or tyrosine residues.[69,70] In our structure of FscN, a well-conserved His53 faces the 8-methyl in

DOI: 10.1021/acs.biochem.5b00354
Biochemistry 2015, 54, 3989−4000

its proximity (3.8 Å) and has no obvious constraints to form a FAD adduct. We have shown that purified holo-FscN is redox-active by the reduction of the enzyme with sodium dithionite, which produced spectra consistent with the formation of $FADH_2$. Efforts to show direct FscN reduction with NADPH or NADH have been unsuccessful in our hands, possibly because of the instability of the reduced flavoenzyme in the absence of substrate. From analysis of the structure and comparison with cocomplex structures of flavoenzyme bound to NADH [highest degree of structural homology, NADH-cytochrome b_5, PDB entry 3W2G (Figure 6)], residues likely involved with NADH binding are present in FscN; however, the very low overall level of structural identity (17% to PDB entry 3W2G) suggests a possible divergent function for FscN. We have made considerable efforts to demonstrate the reduction of various iron chelates with FscN, using the ferrine assay that was previously used to characterize the reduction of YqjH and FchR.[41,45] Unlike FchR, we do not see reduction of "generic" iron chelates as ferric citrate, ferrichrome, or ferric aerobactin. The postulated natural substrate for FscN would be a ferric-fuscachelin A. Although we have access to fuscachelin through isolation from *T. fusca* and through total synthesis, the generation of sufficient quantities of the pure holo-siderophore is a challenge. Regardless, we were able to measure a holo-fuscachelin A reduction activity of 40 nmol of Fe^{2+} min^{-1} mg^{-1}, comparable to that of *E. coli* SIP YqjH (22.0 nmol of Fe^{2+} min^{-1} mg^{-1}). Interestingly, YqjH is a NADPH-dependent reductase, while FscN accepts only NADH. Commonly, the ratio of NAD^+ to NADH inside the cell is high, while the ratio of $NADP^+$ to NADPH is kept low; therefore, bacteria would use NADPH *in vitro* as a reducing agent and NAD^+ as an oxidizing agent. The NADH dependence of FscN may suggest that the siderophore utilization pathway in *T. fusca* has an uncommon redox equilibrium. Additionally, we have demonstrated a 30 μM FscN-ferric fuscachelin A binding affinity, and basic molecular docking calculations using Hexserver[71] suggest that the siderophore may bind the surface of the protein anchored by Glu62 and Asp264 to correspond to the two positively charged D-Arg residues on the siderophore (Figure S7 of the Supporting Information). The pseudosymmetric D-arginines in the natural product (see Figure 1B) are ~25 Å apart, which is approximately the same distance between Glu62 and Asp264 on the protein, suggesting a possible binding mode.

Despite significant effort, we were not able to observe significant direct reduction of flavo-FscN with NADH or NADPH, nor were we successful at reducing a large variety of ferric iron chelates with chemically (sodium dithionate) reduced $FADH_2$–FscN. Structurally, FscN is mostly similar to flavoheme proteins such as cytochrome b_5 reductase that catalyze the transfer of an electron from the two-electron carrier, NADH, to the one-electron carrier, (heme) cytochrome b_5. During iron-siderophore reduction, the terminal electron acceptor (ferric-siderophore) has to be a single-electron acceptor. There is no equivalent heme binding protein near the FscN regulon, and on the basis of the requirement for a single electron reduction step, it is possible the 2Fe-2S cluster of the FSR FscP plays a role in facilitating the transfer of a single electron from NADH to the holo-siderophore. There are multiple known reduction pathways that utilize NAD(P)H, flavin, and Fe_xS_x as components in electron transfer clusters, through *in cis* or *in trans* protein interactions. Additionally, FscN shares 14% sequence identity and structural similarity (rmsd of 3.3 Å) with the 1,2-dioxygenase reductase from *Acinetobacter* sp. (PDB entry 1KRH) (Table S4 of the Supporting Information).[72] Both enzymes have similar NAD(P)H and FAD binding domains, while the dioxygenase reductase has an additional N-terminal 2Fe-2S subdomain for substrate reduction. Another example is the phthalate dioxygenase reductase (PDB entry 2PIA, rmsd of 2.8 Å) that utilizes FMN to mediate the transfer of an electron from the two-electron donor NADH to a [2Fe-2S] single-electron acceptor located on the C-terminus of the protein.[73] In the case of *T. fusca*, electron transfer could proceed from NADH to flavin/FscN to the 2Fe-2S/FscP (or *vice versa*) and then to the iron-siderophore similar to the domain arrangements of other members of flavoprotein reductase families (see Figure S8 of the Supporting Information).[72,74−76] In this scenario, FscP would be in the same position of the iron-porphyrin heme ring as cytochrome b_5 in cytochrome b_5 reductase. Another possibility is that the 2Fe-2S/FscP acts as a holder of a single electron from the flavin semiquinone after a ferric- to ferrous-siderophore reduction. This can allow the ferrous-siderophore to dissociate and a ferric-siderophore to bind followed by the turnover of the flavin semiquinone to complete the stoichiometric reaction.

In the *T. fusca* gene cluster, FscN and FscP are separated by a single gene and are part of the siderophore biosynthesis, transportation, and utilization gene island. This is a unique orientation as compared to those of most bacteria, where the siderophore gene cluster contains only SIP or FSR. For example, in *V. cholerae*, the vibriobactin utilization protein ViuB (SIP) is located next to the nonribosomal peptide synthetase VibF and a FSR-like 2Fe-2S protein is not identified in the organism.[77,78] In *E. coli*, both SIP and FSR homologues can be found in the genome, both with characterized function, but neither is located within a single siderophore biosynthetic regulon. Recently, DtxR has been identified as an iron-dependent transcriptional repressor that regulates the expression of siderophore gene clusters in *T. fusca*.[49] It is possible that the fuscachelin gene cluster is also regulated by the same gene under iron-deficient conditions. Meanwhile, another iron-dependent transcriptional regulator in *T. fusca* TfIdeR binds the toxPO sequence in the presence of a variety of divalent metal ions.[79] Neither of these regulators, however, has been shown to effect transcription of genes in the fuscachelin siderophore cluster. We have conducted initial experiments to assess a potential FscN/FscP protein/protein interaction (see the methods in the Supporting Information and Figure S9 of the Supporting Information). FscN and FscP were co-expressed in a pACYDuet-1 vector with an N-terminal His tag and a C-terminal S tag, respectively. The Ni-NTA resin elution fraction from the co-expression was analyzed via sodium dodecyl sulfate–polyacrylamide gel electrophoresis and His/S tag Western blots. The positive S tag Western blot indicates the prospective protein/protein interaction between FscP and FscN supporting a possible synergistic *in vivo* interaction. Unfortunately, significant efforts to overexpress and purify FscP for *in vitro* analyses and/or structure determination have been unsuccessful in our hands likely because of the significant instability of the holo-iron/sulfur protein.

An intriguing and unexpected aspect of our FscN structure is the observation of a bound metal adjacent to the flavin site. It is not clear if this is an artifact of our purification or crystallization or a natural aspect of the function of FscN. A bound zinc ion that plays a structural role in FscN function is reasonable, but we did observe a surprisingly high molar ratio of nickel ion

DOI: 10.1021/acs.biochem.5b00354
Biochemistry 2015, 54, 3989−4000

bound to FscN, even in the absence of metal affinity purification and a hexa-His tag. Octahedral coordinate Zn^{2+} is rarely observed in protein crystal structures,[80] whereas octahedral Ni^{2+} centers are more common. A relationship exists between nickel ions and the *E. coli* SIP, YqjH. Transcription of the *yqjH* gene is under control of the YqjI transcription factor, a nickel responsive transcriptional repressor.[41] This system and others demonstrate a correlation between iron homeostasis and nickel concentration. There is no apparent *yqjI* homologue in *T. fusca*, and an interesting possibility is that binding of nickel to FscN could play a role in the regulation of enzyme activity. To date, the low *in vitro* reduction activity of FscN has prevented us from testing this hypothesis. In addition, the three histidine residues are not absolutely conserved in SIP members (see Figure 5) and suggest the observed metal binding is likely restricted to a subset of Gram-positive bacteria.

The chemistry and biology of the acquisition of iron by small molecule siderophores is a complex and fascinating process involving metal coordination, protein/protein interactions, and redox chemistry. The specific intercellular fate of the iron-bound siderophore is among the least understood steps at the molecular levels; there are limited examples of direct biochemical demonstration of intracellular iron reduction and transfer to cellular components. The presented structure and biochemical characterization of *T. fusca* FscN provide insight into the role of the SIP family and interplay with siderophores and possibly other protein players, such as FSR. In addition, unexpected structural features and the inability to observe predicted *in vitro* function suggest further investigation into the role of the SIP/FSR family.

■ ASSOCIATED CONTENT

Supporting Information

Supplemental methods for the purification of ferric-siderophore compounds, additional FscN/FscP construct expression and purification, tables of *T. fusca* fuscachelin-related genes and alignments, ICP-MS metal analysis of FscN metal content, figures for fuscachelin/FscN binding ITC analyses and docking, FscN reduction activity determination, S tag/His tag Western blot to probe an FscP/FscN interaction, and a scheme of the domain arrangements of selected flavoprotein reductases. The Supporting Information is available free of charge on the ACS Publications website at DOI: 10.1021/acs.biochem.5b00354.

Accession Codes

The atomic coordinates and the crystallographic structure factors for FscN have been deposited in the Protein Data Bank as entry 4YHB.

■ AUTHOR INFORMATION

Corresponding Author

*Department of Chemistry, University of Florida, P.O. Box 117200, Gainesville, FL 32611. E-mail: bruner@ufl.edu. Telephone: (352) 392-0525.

Funding

We thank the National Science Foundation for supporting this research (CAREER-0645653).

Notes

The authors declare no competing financial interest.

■ ACKNOWLEDGMENTS

We thank Annie Heroux and the staff of beamline X25 at the National Synchrotron Light Source (Brookhaven National Laboratory, Upton, NY) for access and X-ray data collection. Additionally, we thank Prof. Leslie Murray for helpful suggestions and discussions.

■ ABBREVIATIONS

FAD, flavin adenine dinucleotide; NRPs, nonribosomal peptides; SIP, siderophore-interacting protein; FSR, ferric-siderophore reductase; NIS, NRPS-independent siderophore; MFS, major facilitator superfamily; NADH, nicotinamide adenine dinucleotide; NADPH, nicotinamide adenine dinucleotide phosphate; LC−MS, liquid chromatography−mass spectrometry; HPLC, high-pressure liquid chromatography; TFA, trifluoroacetic acid; ITC, isothermal titration calorimetry; DHB, 2,3-dihydroxybenzoic acid; EDTA, ethylenediaminetetraacetic acid; PDB, Protein Data Bank; rmsd, root-mean-square deviation of atomic positions; ICP-MS, inductively coupled plasma mass spectrometry.

■ REFERENCES

(1) Sigel, A., and Sigel, H. (1998) *Iron Transport and Storage in Microorganisms, Plants, and Animals*, Vol. 35, Marcel Dekker, Inc., New York.

(2) Sutak, R., Lesuisse, E., Tachezy, J., and Richardson, D. R. (2008) Crusade for iron: Iron uptake in unicellular eukaryotes and its significance for virulence. *Trends Microbiol. 16*, 261−268.

(3) Kobayashi, T., and Nishizawa, N. K. (2012) Iron uptake, translocation, and regulation in higher plants. *Annu. Rev. Plant Biol. 63*, 131−152.

(4) Weinberg, E. D. (2009) Iron availability and infection. *Biochim. Biophys. Acta 1790*, 600−605.

(5) Miethke, M., and Marahiel, M. A. (2007) Siderophore-based iron acquisition and pathogen control. *Microbiol. Mol. Biol. Rev. 71*, 413−451.

(6) Goetz, D. H., Holmes, M. A., Borregaard, N., Bluhm, M. E., Raymond, K. N., and Strong, R. K. (2002) The neutrophil lipocalin NGAL is a bacteriostatic agent that interferes with siderophore-mediated iron acquisition. *Mol. Cell 10*, 1033−1043.

(7) Sandy, M., and Butler, A. (2009) Microbial iron acquisition: Marine and terrestrial siderophores. *Chem. Rev. 109*, 4580−4595.

(8) Deneer, H. G., Healey, V., and Boychuk, I. (1995) Reduction of exogenous ferric iron by a surface-associated ferric reductase of *Listeria* spp. *Microbiology 141*, 1985−1992.

(9) Tong, Y., and Guo, M. (2009) Bacterial heme-transport proteins and their heme-coordination modes. *Arch. Biochem. Biophys. 481*, 1−15.

(10) Braun, V. (2001) Iron uptake mechanisms and their regulation in pathogenic bacteria. *Int. J. Med. Microbiol. 291*, 67−79.

(11) Raymond, K. N., Dertz, E. A., and Kim, S. S. (2003) Enterobactin: An archetype for microbial iron transport. *Proc. Natl. Acad. Sci. U.S.A. 100*, 3584−3588.

(12) Gründlinger, M., Yasmin, S., Lechner, B. E., Geley, S., Schrettl, M., Hynes, M., and Haas, H. (2013) Fungal siderophore biosynthesis is partially localized in peroxisomes. *Mol. Microbiol. 88*, 862−875.

(13) Furrer, J. L., Sanders, D. N., Hook-Barnard, I. G., and McIntosh, M. A. (2002) Export of the siderophore enterobactin in *Escherichia coli*: Involvement of a 43 kDa membrane exporter. *Mol. Microbiol. 44*, 1225−1234.

(14) Gehring, A. M., Bradley, K. A., and Walsh, C. T. (1997) Enterobactin biosynthesis in *Escherichia coli*: Isochorismate lyase (EntB) is a bifunctional enzyme that is phosphopantetheinylated by EntD and then acylated by EntE using ATP and 2,3-dihydroxybenzoate. *Biochemistry 36*, 8495−8503.

DOI: 10.1021/acs.biochem.5b00354
Biochemistry 2015, 54, 3989−4000

(15) Seyedsayamdost, M. R., Traxler, M. F., Zheng, S., Kolter, R., and Clardy, J. (2011) Structure and biosynthesis of amychelin, an unusual mixed-ligand siderophore from *Amycolatopsis* sp. AA4. *J. Am. Chem. Soc. 133*, 11434−11437.
(16) de Lorenzo, V., and Bindereif, A. (1986) Aerobactin biosynthesis and transport genes of plasmid ColV-K30 in *Escherichia coli* K-12. *J. Bacteriol. 165*, 601−611.
(17) Hider, R. C., and Kong, X. (2010) Chemistry and biology of siderophores. *Nat. Prod. Rep. 27*, 637−657.
(18) Biegel Carson, S. D. B., Klebba, P. E., Newton, S. M. C., and Sparling, P. F. (1999) Ferric enterobactin binding and utilization by *Neisseria gonorrhoeae*. *J. Bacteriol. 181*, 2895−2901.
(19) Wallner, A., Blatzer, M., Schrettl, M., Sarg, B., Lindner, H., and Haas, H. (2009) Ferricrocin, a siderophore involved in intra- and transcellular iron distribution in *Aspergillus fumigatus*. *Appl. Environ. Microbiol. 75*, 4194−4196.
(20) Johnstone, T., and Nolan, E. (2015) Beyond Iron: Non-classical functions of bacterial siderophores. *Dalton Trans.*, 6320−6339.
(21) Bao, G., Clifton, M., Hoette, T. M., Mori, K., Deng, S.-X., Qiu, A., Viltard, M., Williams, D., Paragas, N., Leete, T., Kulkarni, R., Li, X., Lee, B., Kalandadze, A., Ratner, A. J., Pizarro, J. C., Schmidt-Ott, K. M., Landry, D. W., Raymond, K. N., Strong, R. K., and Barasch, J. (2010) Iron traffics in circulation bound to a siderocalin (Ngal)-catechol complex. *Nat. Chem. Biol. 6*, 602−609.
(22) Bobrov, A. G., Kirillina, O., Fetherston, J. D., Miller, M. C., Burlison, J. A., and Perry, R. D. (2014) The *Yersinia pestis* siderophore, yersiniabactin, and the ZnuABC system both contribute to zinc acquisition and the development of lethal septicaemic plague in mice. *Mol. Microbiol. 93*, 759−775.
(23) Jurchen, K. M. C., and Raymond, K. N. (2006) A bidentate terephthalamide ligand, TAMmeg, as an entry into terephthalamide-containing therapeutic iron chelating agents. *Inorg. Chem. 45*, 2438−2447.
(24) Abergel, R. J., and Raymond, K. N. (2011) Multidentate terephthalamidate and hydroxypyridonate ligands: Towards new orally active chelators. *Hemoglobin 35*, 276−290.
(25) Ji, C., Miller, P. A., and Miller, M. J. (2012) Iron transport-mediated drug delivery: Practical syntheses and in vitro antibacterial studies of tris-catecholate siderophore-aminopenicillin conjugates reveals selectively potent antipseudomonal activity. *J. Am. Chem. Soc. 134*, 9898−9901.
(26) Starr, J., Brown, M. F., Aschenbrenner, L., Caspers, N., Che, Y., Gerstenberger, B. S., Huband, M., Knafels, J. D., Lemmon, M. M., Li, C., McCurdy, S. P., McElroy, E., Rauckhorst, M. R., Tomaras, A. P., Young, J. A., Zaniewski, R. P., Shanmugasundaram, V., and Han, S. (2014) Siderophore receptor-mediated uptake of lactivicin analogues in Gram-negative bacteria. *J. Med. Chem. 57*, 3845−3855.
(27) Górska, A., Sloderbach, A., and Marszałł, M. P. (2014) Siderophore-drug complexes: Potential medicinal applications of the "Trojan horse" strategy. *Trends Pharmacol. Sci. 35*, 442−449.
(28) Jones, C. M., Wells, R. M., Madduri, A. V. R., Renfrow, M. B., Ratledge, C., Moody, D. B., and Niederweis, M. (2014) Self-poisoning of *Mycobacterium tuberculosis* by interrupting siderophore recycling. *Proc. Natl. Acad. Sci. U.S.A. 111*, 1945−1950.
(29) Mathavan, I., Zirah, S., Mehmood, S., Choudhury, H. G., Goulard, C., Li, Y., Robinson, C. V., Rebuffat, S., and Beis, K. (2014) Structural basis for hijacking siderophore receptors by antimicrobial lasso peptides. *Nat. Chem. Biol. 10*, 340−342.
(30) Wurst, J. M., Drake, E. J., Theriault, J. R., Jewett, I. T., Verplank, L., Perez, J. R., Dandapani, S., Palmer, M., Moskowitz, S. M., Schreiber, S. L., Munoz, B., and Gulick, A. M. (2014) Identification of inhibitors of PvdQ, an enzyme involved in the synthesis of the siderophore pyoverdine. *ACS Chem. Biol. 9*, 1536−1544.
(31) Garénaux, A., Caza, M., and Dozois, C. M. (2011) The ins and outs of siderophore mediated iron uptake by extra-intestinal pathogenic *Escherichia coli*. *Vet. Microbiol. 153*, 89−98.
(32) Brickman, T. J., and Armstrong, S. K. (2005) *Bordetella* AlcS transporter functions in alcaligin siderophore export and is central to inducer sensing in positive regulation of alcaligin system gene expression. *J. Bacteriol. 187*, 3650−3661.
(33) Stintzi, A., Barnes, C., Xu, J., and Raymond, K. N. (2000) Microbial iron transport via a siderophore shuttle: A membrane ion transport paradigm. *Proc. Natl. Acad. Sci. U.S.A. 97*, 10691−10696.
(34) Dertz, E. A., Stintzi, A., and Raymond, K. N. (2006) Siderophore-mediated iron transport in *Bacillus subtilis* and *Corynebacterium glutamicum*. *JBIC, J. Biol. Inorg. Chem. 11*, 1087−1097.
(35) Chu, B. C. H., Otten, R., Krewulak, K. D., Mulder, F. A. A., and Vogel, H. J. (2014) The solution structure, binding properties, and dynamics of the bacterial siderophore-binding protein FepB. *J. Biol. Chem. 289*, 29219−29234.
(36) Lin, H., Fischbach, M. A., Liu, D. R., and Walsh, C. T. (2005) In vitro characterization of salmochelin and enterobactin trilactone hydrolases IroD, IroE, and Fes. *J. Am. Chem. Soc. 127*, 11075−11084.
(37) Larsen, N. A., Lin, H., Wei, R., Fischbach, M. A., and Walsh, C. T. (2006) Structural characterization of enterobactin hydrolase IroE. *Biochemistry 45*, 10184−10190.
(38) Morton, D. J., Turman, E. J., Hensley, P. D., VanWagoner, T. M., Seale, T. W., Whitby, P. W., and Stull, T. L. (2010) Identification of a siderophore utilization locus in nontypeable *Haemophilus influenzae*. *BMC Microbiol. 10*, 113.
(39) Brickman, T. J., and Mcintosh, M. A. (1992) Overexpression and purification of ferric enterobactin esterase from *Escherichia coli*. *J. Biol. Chem. 267*, 12350−12355.
(40) Miethke, M., Hou, J., and Marahiel, M. A. (2011) The siderophore-interacting protein YqjH acts as a ferric reductase in different iron assimilation pathways of *Escherichia coli*. *Biochemistry 50*, 10951−10964.
(41) Wang, S., Wu, Y., and Outten, F. W. (2011) Fur and the novel regulator YqjI control transcription of the ferric reductase gene yqjH in *Escherichia coli*. *J. Bacteriol.*, 563−574.
(42) Kaplan, C. D., and Kaplan, J. (2009) Iron Acquisition and Transcriptional Regulation. *Chem. Rev. 109*, 4536−4552.
(43) Wang, S., Blahut, M., Wu, Y., Philipkosky, K. E., and Outten, F. W. (2014) Communication between binding sites is required for YqjI regulation of target promoters within the yqjH-yqjI intergenic region. *J. Bacteriol. 196*, 3199−3207.
(44) Matzanke, B. F., Anemüller, S., Schünemann, V., Trautwein, A. X., and Hantke, K. (2004) FhuF, part of a siderophore-reductase system. *Biochemistry 43*, 1386−1392.
(45) Miethke, M., Pierik, A., Peuckert, F., Seubert, A., and Marahiel, M. (2011) Identification and characterization of a novel-type ferric siderophore reductase from a Gram-positive extremophile. *J. Biol. Chem. 286*, 2245−2260.
(46) Dimise, E. J., Widboom, P. F., and Bruner, S. D. (2008) Structure elucidation and biosynthesis of fuscachelins, peptide siderophores from the moderate thermophile *Thermobifida fusca*. *Proc. Natl. Acad. Sci. U.S.A. 105*, 15311−15316.
(47) Dimise, E. J., Condurso, H. L., Stoker, G. E., and Bruner, S. D. (2012) Synthesis and structure confirmation of fuscachelins A and B, structurally unique natural product siderophores from *Thermobifida fusca*. *Org. Biomol. Chem. 10*, 5353−5356.
(48) Lykidis, A., Mavromatis, K., Ivanova, N., Anderson, I., Land, M., DiBartolo, G., Martinez, M., Lapidus, A., Lucas, S., Copeland, A., Richardson, P., Wilson, D. B., and Kyrpides, N. (2007) Genome sequence and analysis of the soil cellulolytic actinomycete *Thermobifida fusca* YX. *J. Bacteriol. 189*, 2477−2486.
(49) Deng, Y., and Zhang, X. (2014) DtxR, an iron-dependent transcriptional repressor that regulates the expression of siderophore gene clusters in *Thermobifida fusca*. *FEMS Microbiol. Lett. 362*, 1−6.
(50) Bamford, V. A., Armour, M., Mitchell, S. A., Cartron, M., Andrews, S. C., and Watson, K. A. (2008) Preliminary X-ray diffraction analysis of YqjH from *Escherichia coli*: A putative cytoplasmic ferri-siderophore reductase. *Acta Crystallogr. F64*, 792−796.
(51) PDB entry 2GPJ. Crystal structure of siderophore-interacting protein (ZP_00813641.1) from *S. putrefaciens* CN-32 at 2.20 Å resolution.
(52) Kabsch, W. (2010) XDS. *Acta Crystallogr. D66*, 125−132.

DOI: 10.1021/acs.biochem.5b00354
Biochemistry 2015, 54, 3989−4000

(53) McCoy, A. J., Grosse-Kunstleve, R. W., Adams, P. D., Winn, M. D., Storoni, L. C., and Read, R. J. (2007) Phaser crystallographic software. *J. Appl. Crystallogr. 40*, 658−674.
(54) Afonine, P. V., Grosse-Kunstleve, R. W., Echols, N., Headd, J. J., Moriarty, N. W., Mustyakimov, M., Terwilliger, T. C., Urzhumtsev, A., Zwart, P. H., and Adams, P. D. (2012) Towards automated crystallographic structure refinement with phenix.refine. *Acta Crystallogr. D68*, 352−367.
(55) Adams, P. D., Afonine, P. V., Bunkóczi, G., Chen, V. B., Davis, I. W., Echols, N., Headd, J. J., Hung, L. W., Kapral, G. J., Grosse-Kunstleve, R. W., McCoy, A. J., Moriarty, N. W., Oeffner, R., Read, R. J., Richardson, D. C., Richardson, J. S., Terwilliger, T. C., and Zwart, P. H. (2010) PHENIX: A comprehensive Python-based system for macromolecular structure solution. *Acta Crystallogr. D66*, 213−221.
(56) Emsley, P., and Cowtan, K. (2004) Coot: Model-building tools for molecular graphics. *Acta Crystallogr. D60*, 2126−2132.
(57) *Pymol: The PyMOL Molecular Graphics System*, version 1.4.1 (2012) Schrödinger, LLC, Portland, OR.
(58) Fox, J. L. (1974) Sodium dithionite reduction of flavin. *FEBS Lett. 39*, 53−55.
(59) Krissinel, E., and Henrick, K. (2007) Inference of macromolecular assemblies from crystalline state. *J. Mol. Biol. 372*, 774−797.
(60) Holm, L., and Rosenström, P. (2010) Dali server: Conservation mapping in 3D. *Nucleic Acids Res. 38*, 545−549.
(61) Yamada, M., Tamada, T., Takeda, K., Matsumoto, F., Ohno, H., Kosugi, M., Takaba, K., Shoyama, Y., Kimura, S., Kuroki, R., and Miki, K. (2013) Elucidations of the catalytic cycle of NADH-cytochrome b5 reductase by X-ray crystallography: New insights into regulation of efficient electron transfer. *J. Mol. Biol. 425*, 4295−4306.
(62) Koder, R. L., and Miller, A. F. (1998) Steady-state kinetic mechanism, stereospecificity, substrate and inhibitor specificity of *Enterobacter cloacae* nitroreductase. *Biochim. Biophys. Acta 1387*, 395−405.
(63) Rane, M. J., and Calvo, K. C. (1997) Reversal of the nucleotide specificity of ketol acid reductoisomerase by site-directed mutagenesis identifies the NADPH binding site. *Arch. Biochem. Biophys. 338*, 83−89.
(64) Petschacher, B., Leitgeb, S., Kavanagh, K. L., Wilson, D. K., and Nidetzky, B. (2005) The coenzyme specificity of *Candida tenuis* xylose reductase (AKR2B5) explored by site-directed mutagenesis and X-ray crystallography. *Biochem. J. 385*, 75−83.
(65) Brinkmann-Chen, S., Flock, T., Cahn, J. K. B., Snow, C. D., Brustad, E. M., McIntosh, J. A., Meinhold, P., Zhang, L., and Arnold, F. H. (2013) General approach to reversing ketol-acid reductoisomerase cofactor dependence from NADPH to NADH. *Proc. Natl. Acad. Sci. U.S.A. 110*, 10946−10951.
(66) Butterton, J. R., and Calderwood, S. B. (1994) Identification, cloning, and sequencing of a gene required for ferric vibriobactin utilization by *Vibrio cholerae*. *J. Bacteriol. 176*, 5631−5638.
(67) McWilliam, H., Li, W., Uludag, M., Squizzato, S., Park, Y. M., Buso, N., Cowley, A. P., and Lopez, R. (2013) Analysis tool web services from the EMBL-EBI. *Nucleic Acids Res. 41*, 597−600.
(68) Söding, J., Biegert, A., and Lupas, A. N. (2005) The HHpred interactive server for protein homology detection and structure prediction. *Nucleic Acids Res. 33*, 244−248.
(69) Mewies, M., McIntire, W. S., and Scrutton, N. S. (1998) Covalent attachment of flavin adenine dinucleotide (FAD) and flavin mononucleotide (FMN) to enzymes: The current state of affairs. *Protein Sci. 7*, 7−20.
(70) Huang, C. H., Lai, W. L., Lee, M. H., Chen, C. J., Vasella, A., Tsai, Y. C., and Liaw, S. H. (2005) Crystal structure of glucooligosaccharide oxidase from *Acremonium strictum*: A novel flavinylation of 6-S-cysteinyl, 8a-N1-histidyl FAD. *J. Biol. Chem. 280*, 38831−38838.
(71) Macindoe, G., Mavridis, L., Venkatraman, V., Devignes, M. D., and Ritchie, D. W. (2010) HexServer: An FFT-based protein docking server powered by graphics processors. *Nucleic Acids Res. 38*, 445−449.
(72) Karlsson, A., Beharry, Z. M., Matthew Eby, D., Coulter, E. D., Neidle, E. L., Kurtz, D. M., Eklund, H., and Ramaswamy, S. (2002) X-ray crystal structure of benzoate 1,2-dioxygenase reductase from *Acinetobacter* sp. strain ADP1. *J. Mol. Biol. 318*, 261−272.
(73) Correll, C. C., Batie, C. J., Ballou, D. P., Ludwig, M. L., Batie, J., Ballou, D. P., Correll, C. C., and Ludwig, M. L. (1992) Phthalate dioxygenase reductase: A modular structure for electron transfer from pyridine nucleotides to [2Fe-2S]. *Science 258*, 1604−1610.
(74) Rosenzweig, A. C., Frederick, C. A., Lippard, S. J., and Nordlund, P. (1993) Crystal structure of a bacterial non-haem iron hydroxylase that catalyses the biological oxidation of methane. *Nature 366*, 537−543.
(75) Senda, M., Kishigami, S., Kimura, S., Fukuda, M., Ishida, T., and Senda, T. (2007) Molecular mechanism of the redox-dependent interaction between NADH-dependent ferredoxin reductase and Rieske-type [2Fe-2S] ferredoxin. *J. Mol. Biol. 373*, 382−400.
(76) Fang, R., Chen, F., Dong, Z., Hu, D., Barbera, A. J., Clark, E. A., Fang, J., Yang, Y., Mei, P., Rutenberg, M., Li, Z., Zhang, Y., Xu, Y., Yang, H., Wang, P., Simon, M. D., Zhou, Q., Li, J., Marynick, M. P., Li, X., Lu, H., Kaiser, U. B., Kingston, R. E., Xu, Y., and Shi, Y. G. (2013) LSD2/KDM1B and its cofactor NPAC/GLYR1 endow a structural and molecular model for regulation of H3K4 demethylation. *Mol. Cell 49*, 558−570.
(77) Butterton, J. R., Choi, M. H., Watnick, P. I., Carroll, P. A., and Calderwood, S. B. (2000) *Vibrio cholerae* VibF is required for vibriobactin synthesis and is a member of the family of nonribosomal peptide synthetases. *J. Bacteriol. 182*, 1731−1738.
(78) Altschup, S. F., Gish, W., Miller, W., Myers, E. W., and Lipman, D. J. (1990) Basic Local Alignment Search Tool. *J. Mol. Biol. 215*, 403−410.
(79) Granger, J. B., Lu, Z., Ferguson, J. B., Santa Maria, P. J., and Novak, W. R. P. (2013) Cloning, expression, purification and characterization of an iron-dependent regulator protein from *Thermobifida fusca*. *Protein Expression Purif. 92*, 190−194.
(80) Patel, K., Kumar, A., and Durani, S. (2007) Analysis of the structural consensus of the zinc coordination centers of metalloprotein structures. *Biochim. Biophys. Acta 1774*, 1247−1253.

DOI: 10.1021/acs.biochem.5b00354
Biochemistry 2015, 54, 3989−4000